# Supporting Information for "Effects of Field-Aligned Cold Plasma Density Filaments on the Fine Structure of Chorus"

M. Hanzelka[1,2], O. Santolík[1,3]

[1]Department of Space Physics, Institute of Atmospheric Physics, Czech Academy of Sciences, Prague, Czech Republic

[2]Center for Space Physics, Boston University, Boston, Massachusetts, USA

[3]Faculty of Mathematics and Physics, Charles University, Prague, Czech Republic

## Contents of this file

1. Text S1

2. Figures S1 to S5

## Introduction

This file contains one short supplementary text describing the parameters of our FDTD simulation scheme, followed by five figures. The first three Figures, S1 to S3, show snapshots of the simulated chorus magnetic wavefield in scenarios with and without ducts. These snapshots help in understanding the propagation paths and attenuation of individual subpackets. The last two figures, S4 and S5, show the waveforms and propagation

Corresponding author: M. Hanzelka (mirekhanzelka@gmail.com)

properties of the chorus element propagating through thin ducts. The placement of probes that recorded the waveforms differs from Figure 4 in the main text. These supporting figures confirm the high variability of the subpacket structure in space.

**Text S1. Parameters of the finite-difference time-domain scheme.**

Unlike Katoh (2014), we limit our investigations to a few degrees of latitude around the magnetic equator, allowing us to use rectilinear coordinates instead of curvilinear without any significant increase in memory demands. The grid size is chosen so that at the equator, across all frequencies of a model wave packet, both parallel and perpendicular wavelengths are resolved by at least 12 points for $\theta_\mathrm{k}$ going up to 75 % of the local resonance cone $\theta_\mathrm{res}(\omega)$. That is,

$$\Delta z \leq 12 \cdot \frac{2\pi}{k_\parallel(\omega, \theta_\mathrm{k})} \quad \forall\, \omega \in [\omega_0, \omega_1],\, \theta_\mathrm{k} \leq \frac{3}{4}\theta_\mathrm{res}(\omega)\,, \tag{1}$$

$$\Delta x \leq 12 \cdot \frac{2\pi}{k_\perp(\omega, \theta_\mathrm{k})} \quad \forall\, \omega \in [\omega_0, \omega_1],\, \theta_\mathrm{k} \leq \frac{3}{4}\theta_\mathrm{res}(\omega)\,, \tag{2}$$

where $k_\parallel$ and $k_\perp$ are the wave vector components, and $\omega_0$ and $\omega_1$ are the lowest and highest wave frequency. Additionally, the characteristic scale length of transverse density irregularities at the equator (see $\sigma_\mathrm{L}$ in Equation 7 of the main text) must be covered by at least 8 points. We tested various finer grids to confirm that our choice produces negligible numerical errors. Finally, to ensure stability, the time step $\Delta t$ was chosen as

$$c\Delta t = \frac{1}{1/\Delta x + 1/\Delta z}\,, \tag{3}$$

which results in a free-space CFL-number between $1/\sqrt{2}$ and 1 for any positive $\Delta x/\Delta z$ ratio (Taflove & Hagness, 2005).

## References

Katoh, Y. (2014, December). A simulation study of the propagation of whistler-mode chorus in the Earth's inner magnetosphere. *Earth Planets Space*, *66*, 6. doi: 10.1186/1880-5981-66-6

Taflove, A., & Hagness, S. C. (2005). *Computational Electrodynamics: The Finite-difference Time-domain Method*. Artech House.

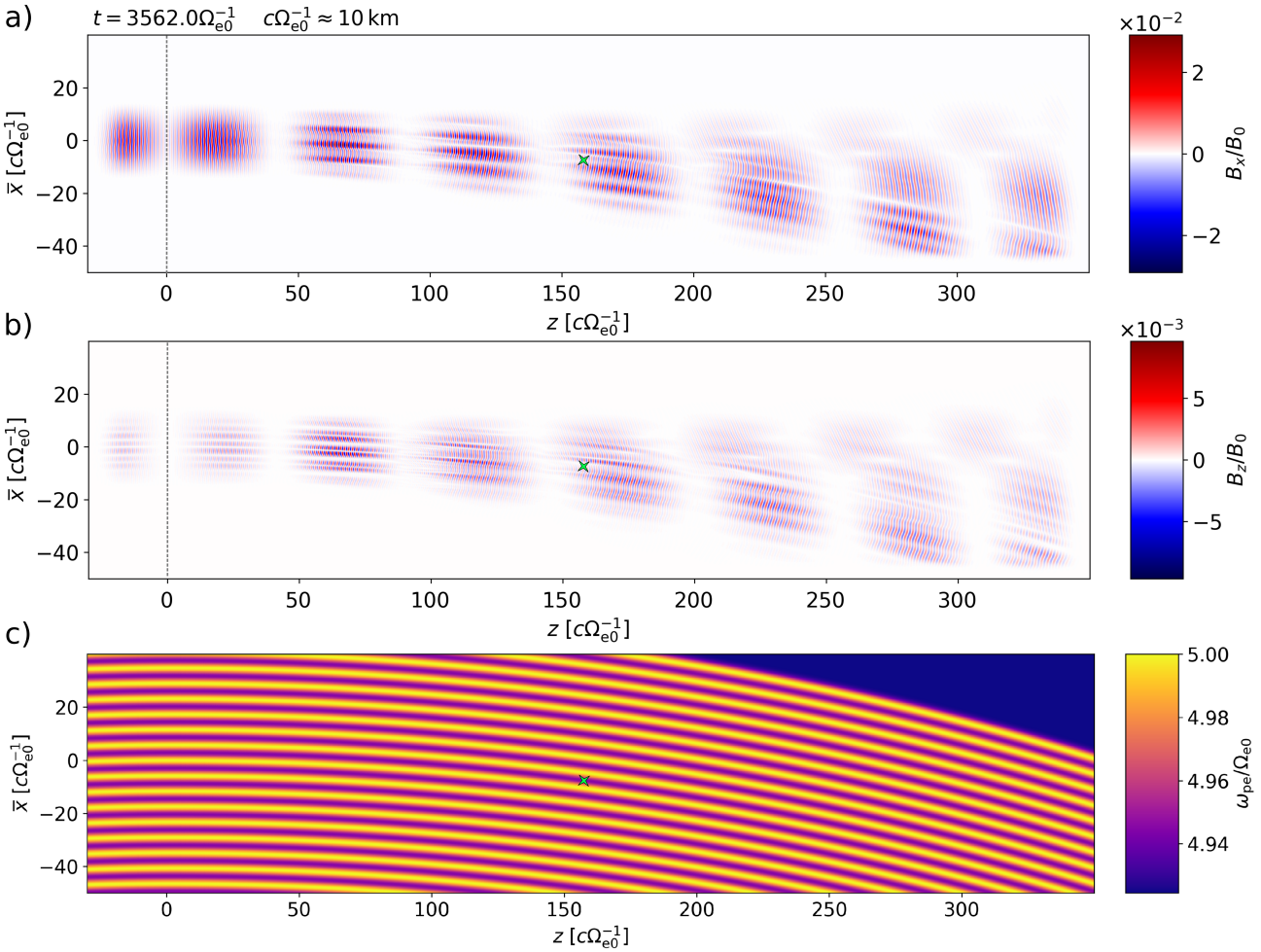


**Figure S1.** Propagation of chorus subpackets in a series of thin, field-aligned density enhancements. a,b) Magnetic field components $B_x$, $B_z$ at time $t = 3562\Omega_{e0}^{-1} \approx 120\,\mathrm{ms}$. We observe that the amplitude becomes focused into individual ducts shortly after leaving the source, with part of the wave becoming unducted and escaping at larger distances. The snapshots were taken after the ninth subpacket was generated. c) Electron plasma frequency $\omega_{pe}$. The green stars mark the position of a probe that recorded the waveforms from Figure 3 in the main text.

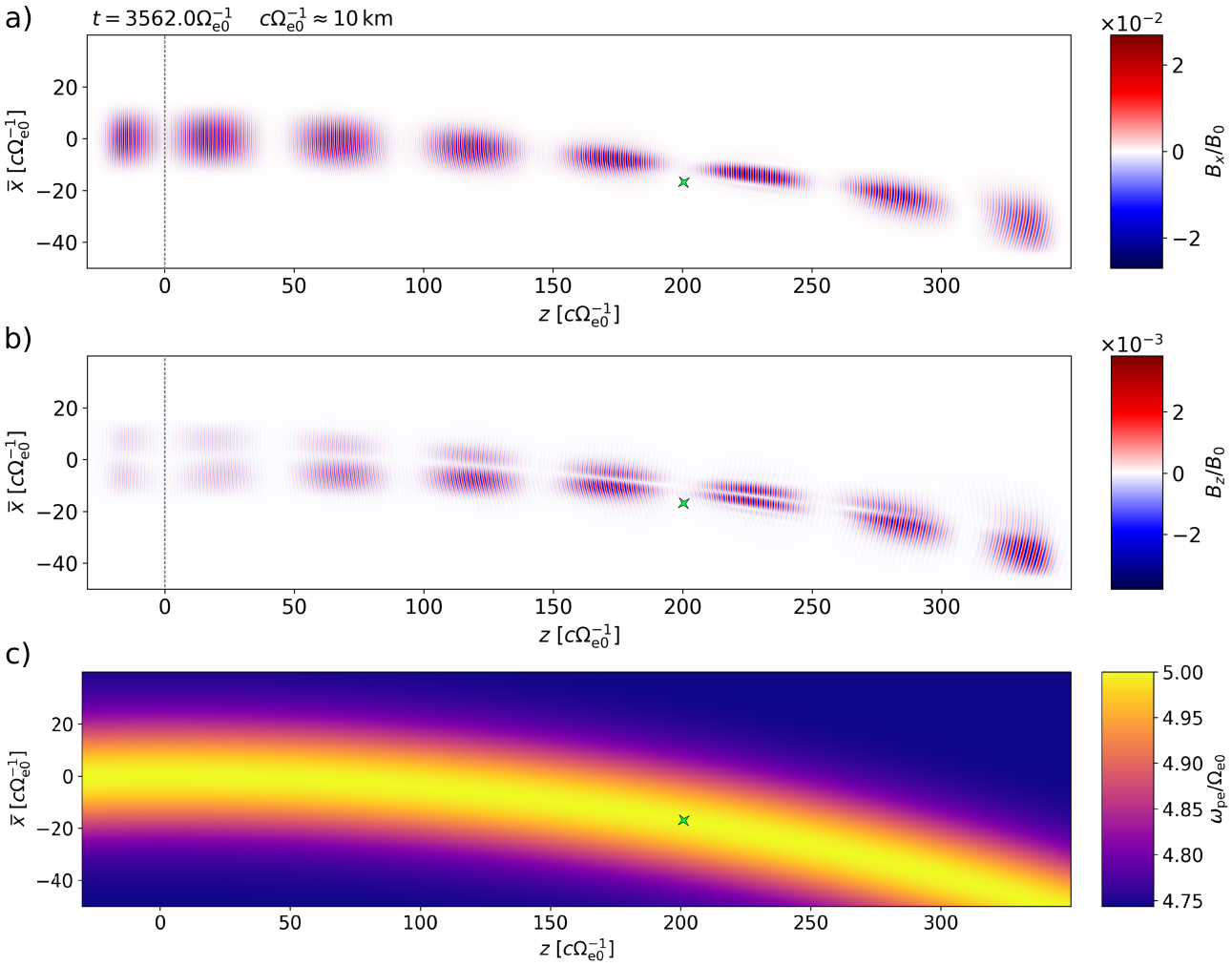


**Figure S2.** Propagation of chorus subpackets in a wide, field-aligned density enhancement. a,b) Magnetic field components $B_x$, $B_z$ at time $t = 3562\Omega_{e0}^{-1} \approx 120\,\mathrm{ms}$, just before the generation of the last (tenth) subpacket. c) Electron plasma frequency $\omega_{pe}$. The green stars mark the position of a probe that recorded the waveforms from Figure 2 in the main text.

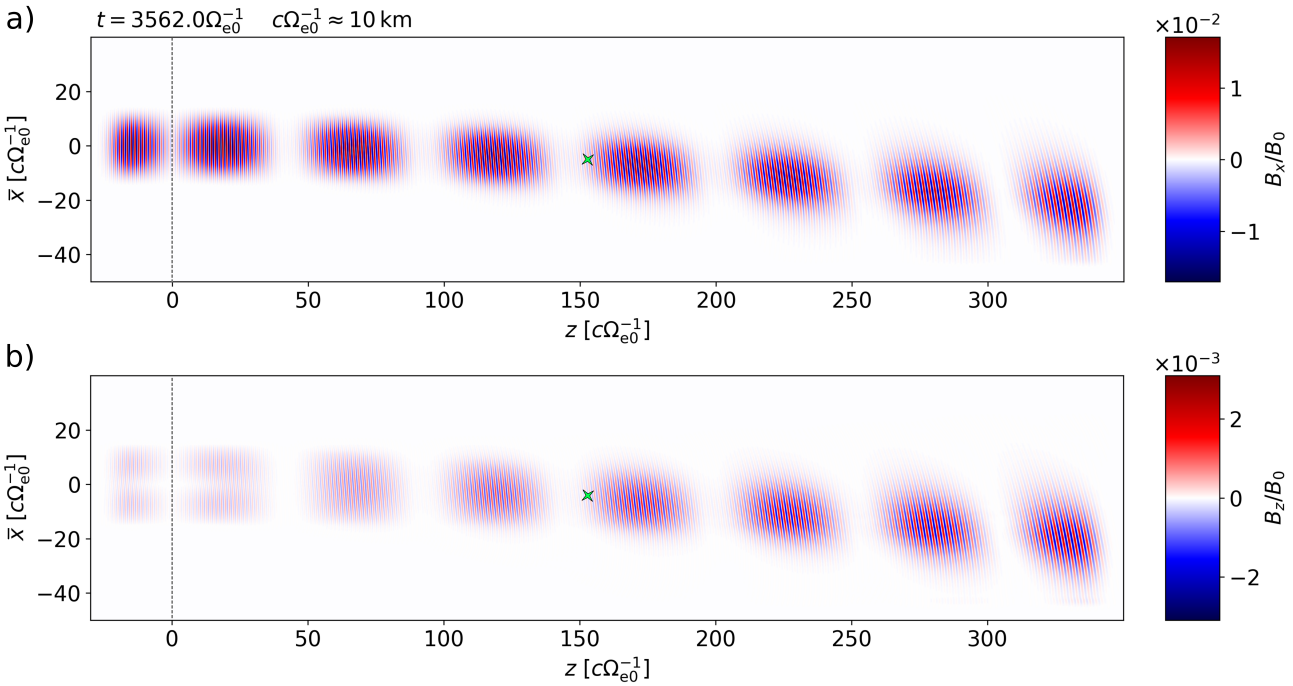


**Figure S3.** Unducted propagation of chorus subpackets. a,b) Magnetic field components $B_x$, $B_z$ at time $t = 3562\Omega_{e0}^{-1} \approx 120$ ms, just before the generation of the last (tenth) subpacket. The green stars mark the position of a probe that recorded the waveforms from Figure 1 in the main text.

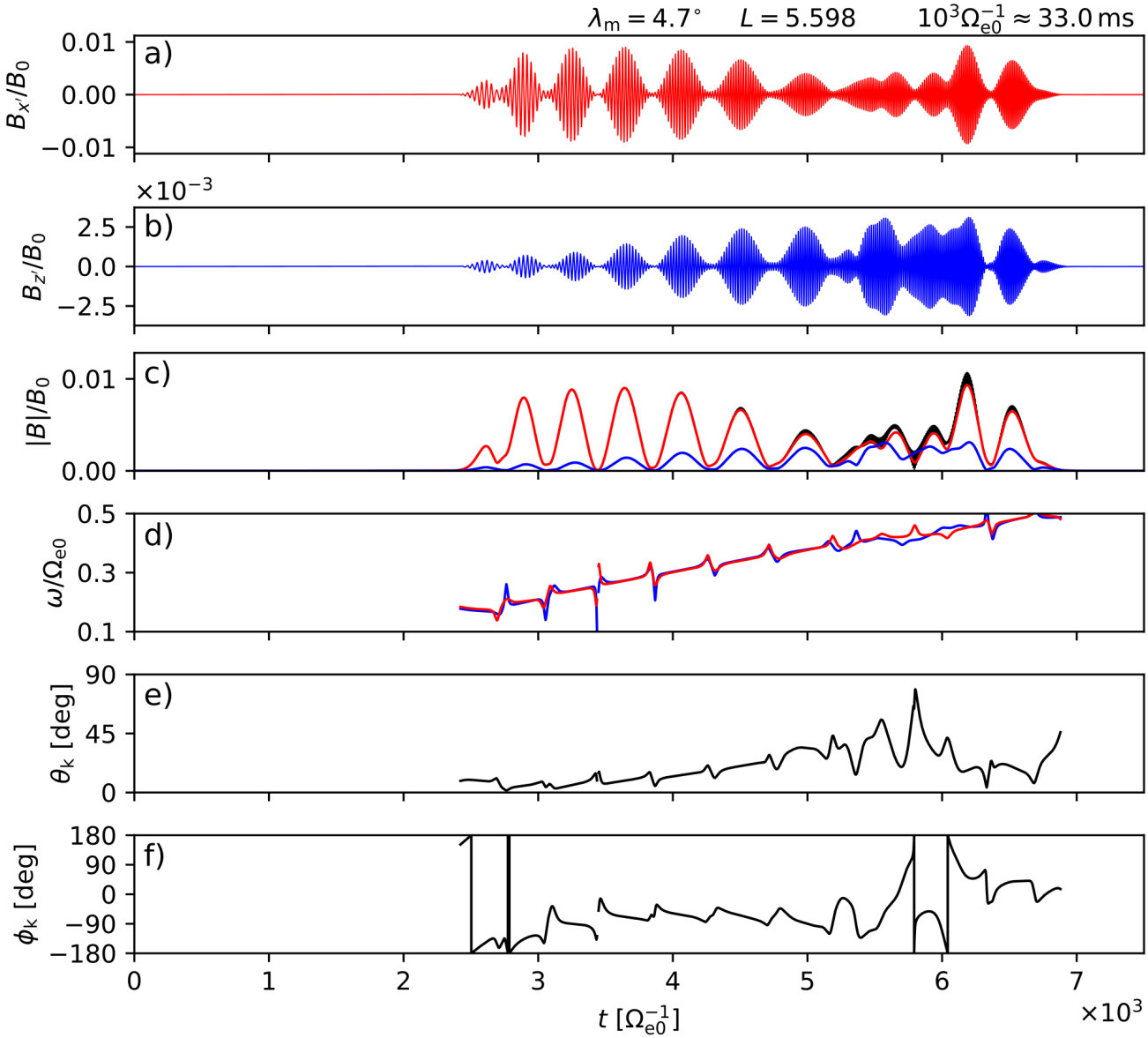


**Figure S4.** Simulated propagation of a lower-band chorus riser with a subpacket structure on a cold plasma density background modulated by a series of thin ducts. The panel format is the same as in Figure 3 of the main text, but the probe was placed further away from the source at $\lambda_m = 4.75°$ and $L = 5.598$ ($-\sigma_L$ from the central field line).

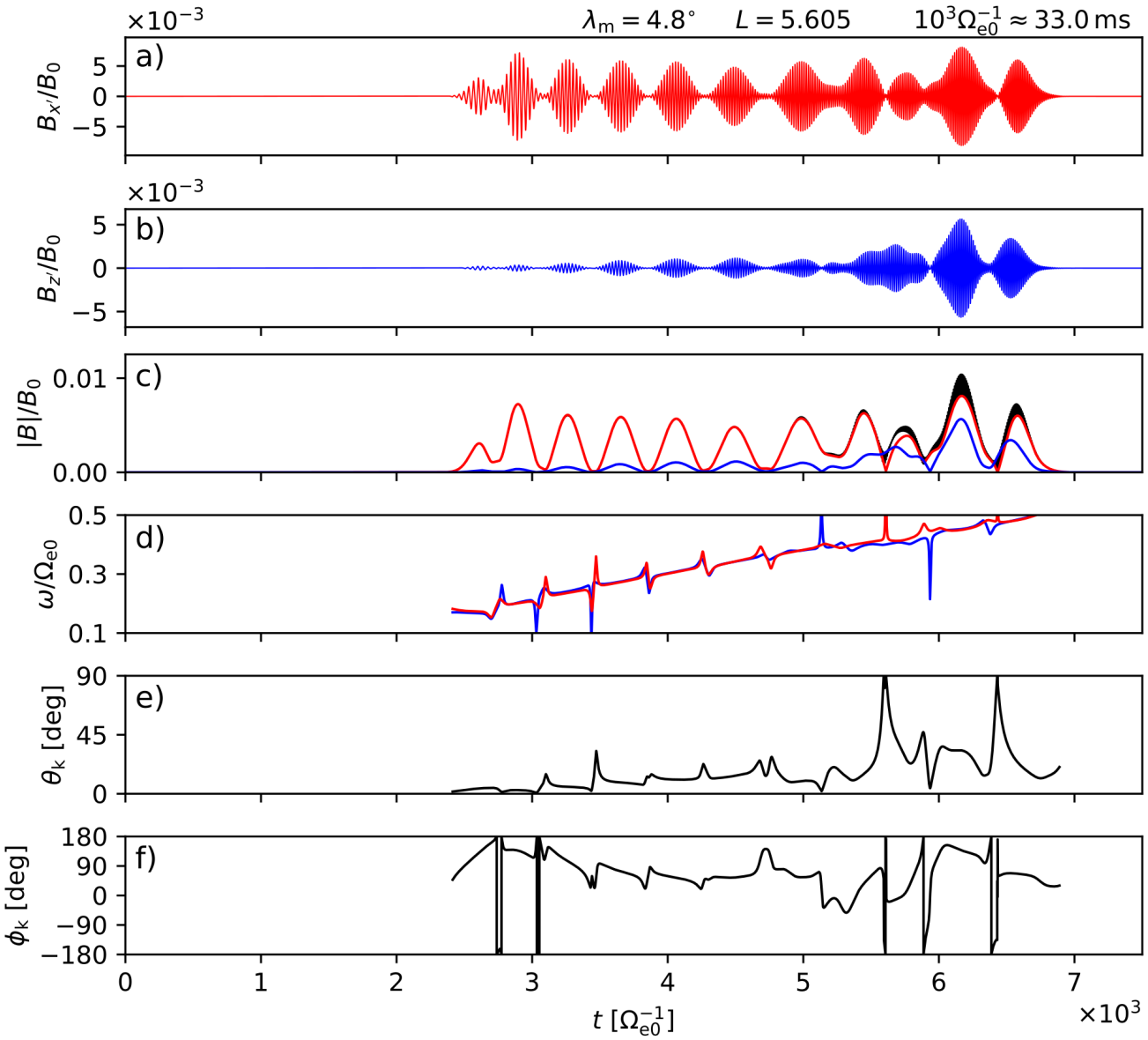


**Figure S5.** Simulated propagation of a lower-band chorus riser with a subpacket structure on a cold plasma density background modulated by a series of thin ducts. The panel format is the same as in Figure 3 of the main text, but the probe was placed further away from the source at $\lambda_m = 4.75°$ and $L = 5.605$ ($+2\sigma_L$ from the central field line). This is the same latitude as in Figure S4, but transverse by position is shifted by $3\sigma_L \approx 43$km. Notice that the subpacket structures differ significantly, especially at higher frequencies.